

Triple-Mode Single-Transistor Graphene Amplifier and Its Applications

Xuebei Yang,^{†,‡} Guanxiong Liu,^{*,‡} Alexander A. Balandin,^{*,*†} and Kartik Mohanram^{†,§,*}

[†]Department of Electrical and Computer Engineering, Rice University, Houston, Texas 77005, United States, [‡]Nano-Device Laboratory, Department of Electrical Engineering and Materials Science and Engineering Program, Bourns College of Engineering, University of California-Riverside, Riverside, California 92521, United States, and

[§]Department of Computer Science, Rice University, Houston, Texas 77005, United States. [‡]These authors contributed equally to this work.

ABSTRACT We propose and experimentally demonstrate a triple-mode single-transistor graphene amplifier utilizing a three-terminal back-gated single-layer graphene transistor. The ambipolar nature of electronic transport in graphene transistors leads to increased amplifier functionality as compared to amplifiers built with unipolar semiconductor devices. The ambipolar graphene transistors can be configured as n-type, p-type, or hybrid-type by changing the gate bias. As a result, the single-transistor graphene amplifier can operate in the common-source, common-drain, or frequency multiplication mode, respectively. This in-field controllability of the single-transistor graphene amplifier can be used to realize the modulation necessary for phase shift keying and frequency shift keying, which are widely used in wireless applications. It also offers new opportunities for designing analog circuits with simpler structure and higher integration densities for communications applications.

KEYWORDS: graphene · transistor · ambipolar · triple-mode amplifier · phase shift keying · frequency shift keying

The single-transistor amplifier, which consists of one transistor and one resistor, is one of the most basic and most important blocks in analog circuits. There are three types of single-transistor amplifiers: common-source, common-drain, and common-gate, each of which exhibits different characteristics. One of the key differences between the three types of amplifiers is determined by the small-signal voltage gain, defined as $\Delta V_{out}/\Delta V_{in}$. The common-source amplifier provides negative gain, whereas the common-drain and common-gate amplifiers provide positive gain. Since different applications usually prefer different types of single-transistor amplifiers, it would be very attractive if the same amplifier can be configured in-field into more than one type. However, in Si-based metal-oxide-semiconductor field-effect transistor (MOSFET) technology, the type of an amplifier is only dependent on its physical configuration, *i.e.*, the node where the input V_{in} is applied, the node where the output V_{out} is obtained, and the placement of the resistor. Therefore, in-field configuration of an amplifier is usually infeasible since

the physical configuration of the amplifier is determined during fabrication.

Recently, graphene, which is a single two-dimensional atomic plane of graphite with a honeycomb crystal lattice, has attracted strong interest as an alternative device technology for future nanoelectronics.^{1–5} Graphene's high carrier mobility, excellent mechanical and thermal stability, superior thermal conductivity,^{6,7} and exceptional resistance to electromigration make graphene an excellent candidate for high-frequency analog applications. Graphene's high carrier mobility can deliver a large small-signal transconductance g_m , defined as $\Delta I_{DS}/\Delta V_{GS}$, which is a key parameter determining the high-frequency performance of a transistor and the gain of an amplifier. Recent work has demonstrated graphene field-effect transistors with a cutoff frequency f_T of 100 GHz,⁸ and it has also been predicted that THz graphene transistors can be achieved at a channel length of 50 nm.⁹ Another important criterion for high-frequency analog applications is an acceptably low level of $1/f$ noise. It was established that graphene transistors produce relatively low levels of $1/f$ noise,^{10–12} comparable to those of conventional semiconductor devices, which makes graphene transistors suitable for analog applications in terms of their noise spectral density.

The most commonly fabricated graphene transistors use intrinsic micrometer-range graphene layers or ribbons as channel material. Owing to the specifics of the band structure of graphene, graphene transistors exhibit the ambipolar current conduction behavior. In the ambipolar transport regime, both hole and electron conduction are feasible depending on

*Address correspondence to balandin@ee.ucr.edu; kmram@rice.edu.

Received for review August 25, 2010 and accepted September 24, 2010.

Published online October 12, 2010. 10.1021/nn1021583

© 2010 American Chemical Society

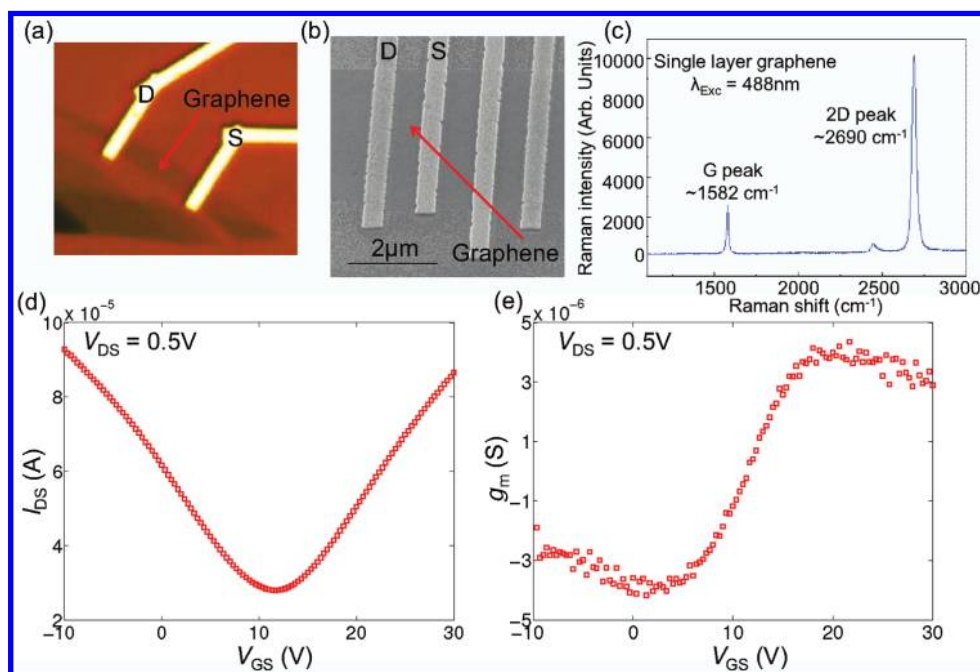


Figure 1. (a) Optical micrograph of a representative fabricated back-gated graphene transistor. (b) SEM image of source and drain electrodes of a representative back-gated graphene transistor. (c) The Raman spectrum of the single-layer graphene. (d) $I_{DS}-V_{GS}$ characteristics of the graphene transistor for $V_{DS} = 0.5$ V. The current is minimum at the Dirac point. (e) g_m-V_{GS} characteristics for $V_{DS} = 0.5$ V. The transconductance g_m is 0 at the Dirac point.

the applied bias.² By properly adjusting the gate-source and drain-source voltages, the transistor can be switched from n-type to p-type, with electron and hole conduction dominating the current, respectively. The ambipolar nature of the charge carrier transport may create problems for conventional applications based on graphene transistors. At the same time, however, it opens up opportunities for increased functionality in nontraditional circuit architectures. For example, graphene transistors have been utilized to demonstrate a frequency multiplier,^{13–15} a functional logic gate,¹⁶ and an inverter.¹⁷ However, these designs either focus on the minimum conduction point of the ambipolar curve where the drain current is at a minimum, which limits the options for design, or require a four-terminal device with a top gate and a back gate that are independently controllable, increasing wiring complexity and operational difficulty.

In this article, we demonstrate a single-transistor amplifier with three modes of operation utilizing the ambipolarity of a three-terminal graphene transistor. Depending on whether the graphene transistor is biased at the left branch, the minimum conduction point, or the right branch of the ambipolar curve, the amplifier will be configured in the common-drain, the frequency multiplier, or the common-source mode of operation. To the best of our knowledge, this is the first demonstration of a single-transistor amplifier that is based on a three-terminal device and that can switch between the common-drain and common-source modes without altering the physical configuration. The proposed triple-mode amplifier is demonstrated using a

three-terminal back-gated graphene transistor. We also show theoretically and experimentally that our graphene amplifier can greatly simplify communications applications such as phase shift keying (PSK) and frequency shift keying (FSK). Compared to conventional designs for these applications, the proposed triple-mode graphene amplifier (i) has a significantly simpler structure, (ii) promises a larger bandwidth and higher frequency of operation, and (iii) promises low power consumption.

To demonstrate the triple-mode graphene amplifier, we have fabricated back-gated graphene transistors from exfoliated graphene flakes. A representative fabricated device, the scanning electron microscope (SEM) image, the Raman spectrum of the single-layer graphene, the $I_{DS}-V_{GS}$ characteristics, and g_m-V_{GS} characteristics are shown in Figure 1a–e. Fabrication and measurement details are provided in the methods section at the end of this article. Strong ambipolar conduction was observed in the graphene transistors as evidenced by the “V”-shaped $I_{DS}-V_{GS}$ curve. In the ambipolar graphene transistor, the transport is dominated by electrons and holes for high and low gate voltages, respectively, and the minimum conduction point V_{min} corresponds to the Dirac point where electrons and holes contribute equally to the transport. The ambipolar graphene transistor should be regarded as n-type or p-type at high gate voltage ($V_{GS} > V_{min}$) or low gate voltage ($V_{GS} < V_{min}$), respectively, and as hybrid-type when the gate voltage is equal to V_{min} . The small-signal transconductance g_m is a key factor

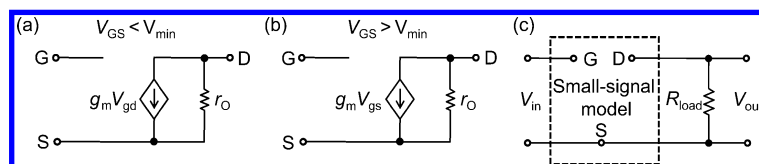


Figure 2. (a,b) Small-signal model for the back-gated graphene transistor, also referred to as the hybrid- π model, under different V_{GS} . Here, g_m is the transconductance and r_o is the output resistance. The small-signal model in panel a is used when $V_{GS} < V_{min}$. Under this condition, the graphene transistor is p-type and the small-signal model is similar to that of a p-type MOSFET.¹⁸ Note that for a p-type MOSFET, the voltage-controlled current source is controlled by V_{gs} , yet in the graphene transistor, it is controlled by V_{gd} . This is because in this paper, we always denote the terminal with higher voltage as the drain for consistency. However, for a p-type MOSFET, the terminal with higher voltage is usually denoted as the source. Therefore, this difference arises completely due to the notation used in this paper. As V_{GS} increases, the back-gated graphene transistor gradually turns from p-type to n-type and the small-signal model in panel b is used when $V_{GS} > V_{min}$. Under this condition, the graphene transistor is n-type and the small-signal model is similar to that of an n-type MOSFET.¹⁸ Note that when V_{GS} is close to V_{min} , the graphene transistor should be considered as hybrid-type instead of either n-type or p-type. Therefore, neither the n-type nor the p-type small-signal model is suitable to describe the performance of the graphene transistor. In panel c, we present the circuit for small-signal analysis of the triple-mode graphene amplifier from Figure 3a. Note that in small-signal circuit analysis, the power supply is shorted and the nodes for V_{DD} and ground are replaced by a single reference.

dominating the high-frequency performance of a transistor and the gain of the amplifier. As shown in Figure 1e, g_m is positive when $V_{GS} > V_{min}$ and negative when $V_{GS} < V_{min}$, reflecting electron current and hole current, respectively.

The small-signal model for the back-gated graphene transistor, also referred to as the hybrid- π model, under different V_{GS} is shown in Figure 2 panels a and b. Here, r_o is the output resistance and g_m is the small-signal transconductance of the graphene transistor. Since the graphene transistor is p-type when $V_{GS} < V_{min}$, the small-signal model is similar to that of a p-type MOSFET¹⁸ in Figure 2a. Note that for a p-type MOSFET, the voltage-controlled current source is controlled by V_{gs} , yet in the graphene transistor, it is controlled by V_{gd} . This is because in this paper, we always denote the terminal with higher voltage as the drain for consistency. However, for a p-type MOSFET, the terminal with higher voltage is usually denoted as the source. Therefore, this difference arises completely due to the notation used in this paper. Since the transistor is n-type when $V_{GS} > V_{min}$, the small-signal model is similar to that of an n-type MOSFET¹⁸ in Figure 2b. For V_{GS} close to V_{min} , the graphene transistor should be considered as hybrid-type instead of either n-type or p-type. Therefore, neither the n-type nor the p-type small-signal model is suitable to describe the performance of the graphene transistor. Finally, Figure 2c illustrates the circuit for small-signal analysis of the triple-mode graphene amplifier, which will be introduced in the next section.

Since conventional circuit design has been based on unipolar devices wherein only one type of carrier dominates the conduction, ambipolar conduction has usually been considered undesirable. However, our work is inspired by the ability to leverage the ambipolarity of graphene transistors during circuit operation.

TRIPLE-MODE AMPLIFIER

In this work, we build a triple-mode single-transistor amplifier using a single back-gated graphene transis-

tor and an off-chip resistor. The schematic of the graphene amplifier is shown in Figure 3a. The supply voltage V_{DD} is set to 1 V, and the resistor R_{load} is 20 k Ω . V_{bias} is a fixed DC voltage and V_{ac} is a small sinusoidal AC signal. The gate-source voltage of the graphene transistor is hence equal to $V_{bias} + V_{ac}$. We show that depending on the relationship between V_{bias} and the Dirac point V_{min} , this amplifier can have three modes of operation. In each mode, the amplifier exhibits different performance in terms of the small-signal voltage gain $\Delta V_{out}/\Delta V_{in}$, which is given by the expression $\Delta(V_{DD} - I_{DS}R_{load})/\Delta V_{in}$.

Mode 1 $V_{bias} < V_{min}$. When $V_{bias} < V_{min}$, the transistor is biased at the left branch of the ambipolar conduction curve, so the small-signal transconductance g_m of the transistor is negative. In the positive phase of V_{ac} , I_{DS} decreases as V_{GS} increases. As a result, the voltage drop across the resistor decreases and V_{out} increases. It can be similarly inferred that in the negative phase of V_{ac} , V_{out} will decrease. Therefore, the small-signal voltage gain in mode 1 is positive, and the input and the output signals have the same phase. From the transport perspective, when $V_{bias} < V_{min}$, the current is mainly due to hole conduction, so the transistor can be regarded as p-type. Under this condition, the circuit is configured as a common-drain amplifier. Analytically, the gain of the amplifier in this mode is given by the expression $|g_m|R_{total}/(|g_m|R_{total} + 1)$, where R_{total} is the parallel combination of the load resistor R_{load} and the inherent output resistance r_o of the graphene transistor. This expression can be derived from the small-signal analysis of the complete circuit illustrated in Figure 2c, using the small-signal model for the graphene transistor shown in Figure 2a. The measured results for mode 1 is presented in Figure 3c. The applied bias voltage V_{bias} is 6.5 V and the frequency of the input AC signal V_{ac} is 10 kHz.

Mode 2 $V_{bias} > V_{min}$. When $V_{bias} > V_{min}$, the transistor is biased at the right branch of the ambipolar conduction curve, so the small-signal transconductance g_m of the transistor is positive. In the positive phase of V_{ac} , I_{DS}

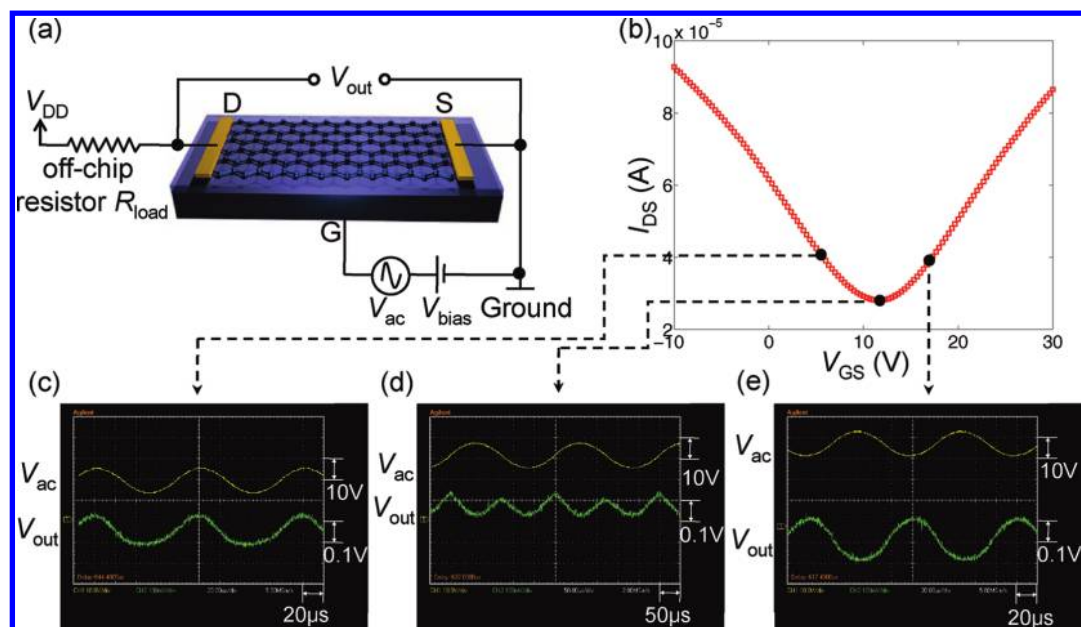


Figure 3. (a) The schematic for the triple-mode single-transistor graphene amplifier based on an off-chip resistor R_{load} . (b) The $I_{DS}-V_{GS}$ characteristics of the graphene transistor. The three dots represent three representative bias voltages for the three different modes of operation. From the left to the right, for the three bias voltages, the amplifier is configured in the common-drain mode, the frequency multiplication mode, and the common-source mode, respectively. (c) The AC coupled input and output signals when the amplifier is biased at the left branch of the ambipolar curve. In this configuration, the amplifier is in the common-drain mode, and the output signal has the same frequency and phase as the input signal. (d) The AC coupled input and output signals when the amplifier is biased at the Dirac point. In this configuration, the amplifier is in the frequency multiplication mode, and the frequency of the output signal is doubled as compared to that of the input signal. (e) The AC coupled input and output signals when the amplifier is biased at the right branch of the ambipolar curve. In this configuration, the amplifier is in the common-source mode, and the output signal has the same frequency but a 180° phase shift as compared to the input signal.

increases as V_{GS} increases. As a result, the voltage drop across the resistor increases and V_{out} decreases. It can be similarly inferred that in the negative phase of V_{acr} V_{out} will increase. Therefore, the small-signal voltage gain in mode 2 is negative, and the output signal will exhibit a phase shift of 180° with respect to the input signal. From the transport perspective, when $V_{bias} > V_{min}$, the current is mainly due to electron conduction, so the transistor can be regarded as n-type. Under this condition, the circuit is configured as a common-source amplifier. Analytically, the gain of the amplifier in this mode is given by the expression $-|g_m|R_{total}$, where R_{total} is the parallel combination of R_{load} and r_o . As in mode 1, this expression can be derived from the small-signal analysis of the complete circuit illustrated in Figure 2c, using the small-signal model for the graphene transistor shown in Figure 2b. The measured results for mode 2 is presented in Figure 3e. The applied bias voltage V_{bias} is 17.5 V and the frequency of the input AC signal V_{ac} is 10kHz.

Mode 3 $V_{bias} = V_{min}$. When $V_{bias} = V_{min}$, the transistor is biased at the minimum conduction point. In the positive phase of V_{acr} , the small-signal transconductance is positive. As a result, the small-signal voltage gain is negative, as analyzed in mode 2. In contrast, in the negative phase of V_{acr} , the small-signal transconductance is negative. As a result, the small-signal voltage gain of the amplifier is positive, as analyzed in mode 1.

Thus, when V_{bias} is equal to V_{min} , the input signal sees a positive gain in its positive phase and a negative gain in its negative phase, resulting in frequency doubling. The measured results for mode 3 is presented in Figure 3d. The applied bias voltage V_{bias} is 11.1 V and the frequency of the input AC signal V_{ac} is 4kHz. The spectral purity of the obtained output was analyzed using the fast Fourier transform. Frequency doubling effect is clearly observed since it is observed that 83% of energy of the output signal is at the frequency of 8kHz. This effect has also been previously reported.¹³

The proposed single-transistor graphene amplifier utilizes the key concept of biasing in analog circuits, that is, only a small range of $I-V$ characteristics near the bias point are necessary to optimize the circuit performance. For this reason, ambipolar conduction can provide a larger design-space than unipolar conduction because of the richer diversity of $I-V$ characteristics. Compared to the traditional amplifiers based on unipolar devices, the proposed single-transistor amplifier provides greater in-field controllability as it can switch between the three modes during operation. To the best of our knowledge, this is the first work to demonstrate that a single-transistor amplifier based on a three-terminal device can be in-field configured to function as both a common-source and a common-drain amplifier. The small-signal gain observed in the three modes of operation is $\approx 0.01-0.02$, which is con-

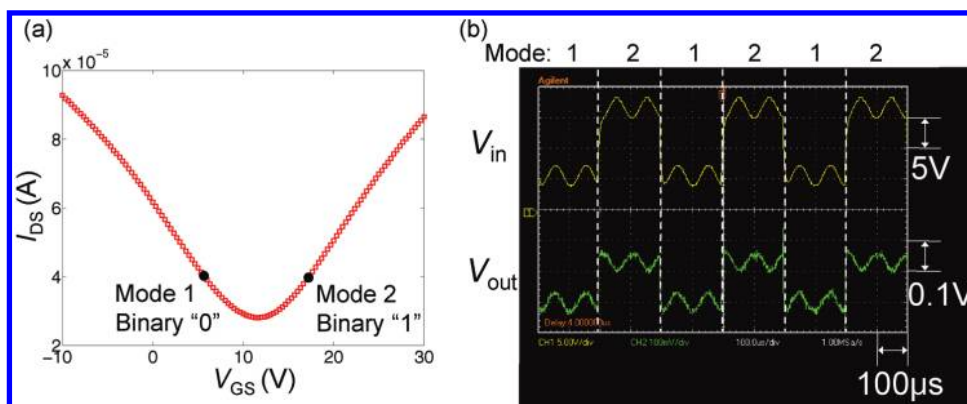


Figure 4. (a) Two bias voltages, 5.83 and 16.8 V, represent “0” and “1”. (b) Experimental results for BPSK modulation. Note that when the bias voltage is 5.83 V, the amplifier is configured in mode 1 and the output signal has the same phase as the input signal. When the bias voltage is 16.8 V, however, the amplifier is configured in mode 2 and the output signal has a phase shift of 180° as compared to the input signal.

sistent with the small-signal gain that has been reported for graphene transistors in literature.^{13,14,17} The low gain can be attributed to the immaturity of the fabrication techniques common to all graphene devices. In this article, we demonstrate that the proposed single-transistor triple-mode amplifier can greatly simplify circuits in common communications applications such as PSK and FSK. Both PSK and FSK are important digital modulation techniques. PSK is widely used in wireless applications such as Bluetooth, radio frequency identification (RFID), and Zig-Bee, while FSK is often used in audio and radio systems.¹⁹

APPLICATIONS

We first consider the application of PSK. For brevity, we consider binary PSK (BPSK) that is the most basic variant of PSK in this article, but the idea can be extended to other forms of PSK such as quadrature PSK (QPSK). In BPSK, the phase of the small AC carrier signal is modulated and shifted between 0° and 180° to represent the data stream, which takes the binary value of (0,1). By using the triple-mode amplifier, BPSK modulation can be achieved by applying the sinusoid carrier as the small AC signal V_{ac} and the data stream, which is the large square wave signal, as the bias V_{bias} . If the swing of the square wave signal V_{bias} is chosen such that the amplifier can be switched between the positive-gain and negative-gain modes, the carrier signal will either experience no phase shift or a phase shift of 180° . The experimental results for BPSK modulation is presented in Figure 4. The biasing voltage V_{bias} is switched between 5.83 and 16.8 V, representing digital data “0” and “1”, respectively. It is generated as a square wave signal from the signal generator. When V_{bias} is 5.83 V, the graphene transistor is biased at the left branch, so the amplifier operates in mode 1 with a positive gain. When V_{bias} is 16.8 V, the graphene transistor is biased at the right branch, so the amplifier operates in mode 2 with a negative gain. The frequency of V_{ac} is 10 kHz. Note that the output signal has different DC

voltages when the amplifier is configured in mode 1 and mode 2, which may not be preferred during demodulation. However, the DC voltage can be easily filtered out using a high-pass filter.

We next consider binary FSK (BFSK) that is the most basic variant of FSK for illustration. In BFSK, the frequency of the small AC carrier signal is modulated and shifted between f_{c1} and f_{c2} to represent the data stream, which takes the binary value of (0,1). If $f_{c2} = 2f_{c1}$, such as in the case of Kansas City standard (KCS) for audio cassette drives where $f_{c1} = 1200$ Hz and $f_{c2} = 2400$ Hz, BFSK modulation can be successfully achieved using the proposed triple-mode amplifier. Again, as in the case of BPSK, we can apply the sinusoid carrier as a small AC signal and the data stream, which is the large square wave signal, as the bias. If the square wave signal V_{bias} is chosen such that the amplifier is biased in mode 3 or in either mode 1/mode 2, the frequency of the output signal will either be doubled or remain the same, realizing BFSK. The experimental results for BFSK modulation is presented in Figure 5. The biasing voltage V_{bias} , generated as a square wave signal from the signal generator is switched between 11.1 and 21.9 V, representing digital data “0” and “1”, respectively. When V_{bias} is 11.1 V, the graphene transistor is biased at the Dirac point V_{min} , so the amplifier operates in mode 3. When V_{bias} is 21.9 V, the graphene transistor is biased at the right branch, so the amplifier operates in mode 2 with a negative gain. The problem of mismatched DC voltage at the output can be similarly solved by using a high-pass filter.

For comparison, traditional PSK and FSK modulation is usually achieved using analog multipliers that require multiple transistors and/or filtering devices. However, by leveraging the ambipolar conduction, the proposed amplifier provides a single-transistor design to achieve PSK and FSK modulation. It greatly simplifies the circuit design and the simple structure will potentially also lower power consumption. Note that the concept described in this article also applies to other ma-

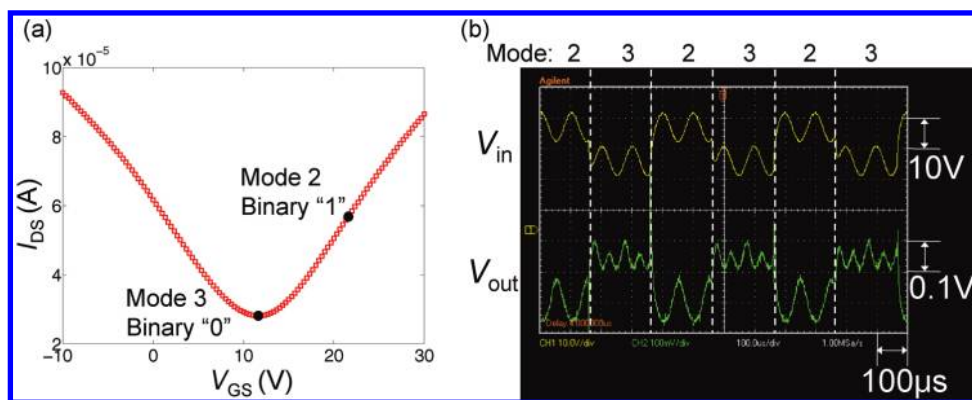


Figure 5. (a) Two bias voltages, 11.1 and 21.9 V, represent “0” and “1”. (b) Experimental results for BFSK modulation. Note that when the bias voltage is 11.1 V, the amplifier is configured in mode 3 and the frequency of the output signal is doubled in comparison to the input signal. When the bias voltage is 21.9 V, however, the amplifier is configured in mode 2 and the output signal has the same frequency as the input signal.

materials exhibiting ambipolar conduction properties, such as silicon nanowires,²⁰ organic semiconductor heterostructures,²¹ and carbon nanotubes (CNTs).²² Among these materials, both CNTs and graphene have high mobility that is preferable for high-frequency analog applications. However, the two-dimensional planar structure of graphene enables the current to be easily increased by increasing the width of the graphene channel, which is advantageous over CNT transistors.

Given the excellent advantages of the triple-mode amplifier, there are several directions that merit further investigation to optimize its performance. Currently, the gain of the amplifier is low and of the order of 0.01–0.02. This is because (i) the graphene transistor exhibits low small-signal transconductance g_m and (ii) the transistor operates in the linear region, with a small inherent output resistance r_o . We believe that this problem can be solved by improving the device structure and channel quality, increasing the g_m , and pushing the transistor into the saturation region. Indeed, a frequency multiplier (mode 3 application of the triple-mode amplifier) with a small-signal gain of 0.15 has been recently reported using the relatively mature CNT.¹⁵ Another challenge is the mismatch in gain between the different modes for applications such as PSK and FSK, which may result in extra power loss and higher bit-error rate. We anticipate that the mismatch will increase as the gain increases. We believe that the mismatch results from (i) asymmetry in the I – V characteristics between the left and the right branch of the ambipolar curve and (ii) the inherent performance differences between the common-source and the common-drain amplifier. Asymmetry between the electron and hole branches can be reduced by improving the cleanliness of the sample. For example, e-beam resist residue that is present in the fresh fabricated devices can be removed by annealing the device in Ar/ H_2 .²³ Inherent performance differences between the different modes of operation can be reduced by introducing feedback and using differential outputs. One

such circuit structure is presented in Figure 6. For this structure, if $R_1 = R_2$, the circuit is symmetric when the transistor is biased at the left and the right branch, and balanced gains can be achieved. Since the currently achievable gain is small in all the modes of operation, the benefits of the proposed differential structure are not experimentally observable. However, we have validated this design using circuit simulations and we believe that such differential designs will become effective as the gain increases. Other nonidealities in the output signal such as distortions and glitches exist, but we believe that they can be addressed by improving the quality of the graphene transistor.

CONCLUSIONS

We propose and experimentally demonstrate a triple-mode single-transistor graphene amplifier in this article. The graphene amplifier was built using a three-terminal back-gated single-layer graphene transistor and an off-chip resistor. The ambipolarity of charge transport in graphene is an essential element for the triple-mode operation of the amplifier. Depending on the bias voltage, the amplifier can be configured in either the common-source, common-drain, or frequency multiplication mode of operation. To the best of our knowledge, this is the first demonstration of a single-transistor amplifier that can be tuned between the common-source and common-drain configuration using a single three-terminal transistor. We also experimentally demonstrated that the in-field controllability can be used to realize the modulation necessary for phase shift key-

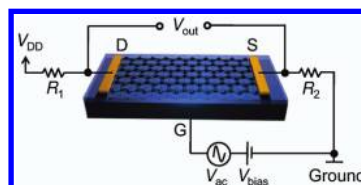


Figure 6. Circuit structure utilizing feedback and differential output to reduce the performance difference between the different modes of operation.

ing and frequency shift keying in communications circuits. As progress is made in graphene-based thin films for transparent and printable electronics, such

simple circuits deliver both high functionality and in-field configuration capability necessary for large-scale integration and commercialization.

METHODS

Graphene Transistor Fabrication. In this work, the back-gated graphene transistor is fabricated using the following methods. Graphene flakes were placed on a standard silicon substrate with 300 nm SiO₂ on the top. The number of atomic layers and quality of graphene flakes were verified by micro-Raman spectroscopy through the conventional procedure of the 2D/G' Raman-band deconvolution.^{24–26} The p-type degenerately doped Si substrate was used as the back gate to tune the Fermi-level position of graphene. The source and drain electrodes were fabricated by electron beam lithography (EBL) followed by the electron beam evaporation of Ti/Au with the thickness of 8/80 nm. The channel width of the fabricated devices was 2 μm and the length was 9 μm. The DC electrical characteristics of the fabricated graphene transistors were measured by the probe station (Agilent 4142) under ambient conditions.²⁷ The gate biases ranging from –10 to 30 V were applied for the back gate measurements at a fixed drain bias of 0.5 V. The I_{ON}/I_{OFF} ratio was around 3, while the charge carrier mobility of these devices was in the range 3000–4000 cm² V^{–1} s^{–1} at room temperature.

Triple-Mode Amplifier Circuit Setup. The schematic of the graphene amplifier is shown in Figure 3a. V_{bias} is a fixed DC voltage and V_{ac} is a small sinusoidal AC signal. The input and output voltages of the triple-mode single-transistor graphene amplifier are measured using an oscilloscope (Agilent DSO3102A). V_{bias} and V_{DD} are applied using a power supply (Kepco ABC 40–0.5), and V_{ac} is applied using a signal generator (GM Instek GFG 8020H).

Acknowledgment. The work at Rice University was supported by NSF Grant CCF-0916636. The work at the University of California–Riverside was supported by the DARPA–SRC Focus Center Research Program (FCRP) through its Center on Functional Engineered Nano Architectonics (FENA).

REFERENCES AND NOTES

- Novoselov, K. S.; Geim, A. K.; Morozov, S. V.; Jiang, D.; Zhang, Y.; Dubonos, S. V.; Grigorieva, I. V.; Firsov, A. A. Electric Field Effect in Atomically Thin Carbon Films. *Science* **2004**, *306*, 666–669.
- Geim, A.; Novoselov, N. The Rise of Graphene. *Nat. Mater.* **2007**, *6*, 183–191.
- Li, X.; Wang, X.; Zhang, L.; Lee, S.; Dai, H. Chemically Derived, Ultrasoft Graphene Nanoribbon Semiconductors. *Science* **2008**, *319*, 1229–1232.
- Avouris, P.; Chen, Z.; Perebeinos, V. Carbon-Based Electronics. *Nat. Nanotechnol.* **2007**, *2*, 605–615.
- Meric, I.; Han, M. Y.; Young, A. F.; Ozyilmaz, B.; Kim, P.; Shepard, K. L. Current Saturation in Zero-Bandgap, Top-Gated Graphene Field-Effect Transistors. *Nat. Nanotechnol.* **2008**, *3*, 654–659.
- Balandin, A. A.; Ghosh, S.; Bao, W.; Calizo, I.; Teweldebrhan, D.; Miao, F.; Lau, C. Superior Thermal Conductivity of Single-Layer Graphene. *Nano Lett.* **2008**, *8*, 902–907.
- Ghosh, S.; Bao, W.; Nika, D. L.; Subrina, S.; Pokatilov, E.; Lau, C.; Balandin, A. A. Dimensional Crossover of Thermal Transport in Few-Layer Graphene. *Nat. Mater.* **2010**, *9*, 555–558.
- Lin, Y.-M.; Dimitrakopoulos, C.; Jenkins, K. A.; Farmer, D. B.; Chiu, H.-Y.; Grill, A.; Avouris, P. 100-GHz Transistors from Wafer-Scale Epitaxial Graphene. *Science* **2010**, *327*, 662.
- Lin, Y.; Jenkins, K. A.; Valdes-Garcia, A.; Small, J. P.; Farmer, D. B.; Avouris, P. Operation of Graphene Transistors at Gigahertz Frequencies. *Nano Lett.* **2009**, *9*, 422–426.
- Lin, Y.-M.; Avouris, P. Strong Suppression of Electrical Noise in Bilayer Graphene Nanodevices. *Nano Lett.* **2008**, *8*, 2119–2125.
- Shao, Q.; Liu, G.; Teweldebrhan, D.; Balandin, A. A.; Romyantsev, S.; Shur, M.; Yan, D. Flicker Noise in Bilayer Graphene Transistors. *IEEE Electron Device Lett.* **2009**, *30*, 288–290.
- Liu, G.; Stillman, W.; Romyantsev, S.; Shao, Q.; Shur, M.; Balandin, A. A. Low-Frequency Electronic Noise in the Double-Gate Single-Layer Graphene Transistors. *Appl. Phys. Lett.* **2009**, *95*, 033103.
- Wang, H.; Nezhich, D.; Kong, J.; Palacios, T. Graphene Frequency Multipliers. *IEEE Electron Device Lett.* **2009**, *30*, 547–549.
- Wang, Z.; Zhang, Z.; Xu, H.; Ding, L.; Wang, S.; Peng, L.-M. A High-Performance Top-Gate Graphene Field-Effect Transistor Based Frequency Doubler. *Appl. Phys. Lett.* **2010**, *96*, 173104.
- Wang, Z.; Ding, L.; Pei, T.; Zhang, Z.; Wang, S.; Yu, T.; Ye, X.; Peng, F.; Li, Y.; Peng, L. M. Large Signal Operation of Small Band-Gap Carbon Nanotube-Based Ambipolar Transistor: A High-Performance Frequency Doubler. *Nano Lett.* **2010**, *10*, 3648–3655.
- Sordan, R.; Traversi, F.; Russo, V. Logic Gates with a Single Graphene Transistor. *Appl. Phys. Lett.* **2009**, *94*, 073305.
- Harada, N.; Yagi, K.; Sato, S.; Yokoyama, N. A Polarity-Controllable Graphene Inverter. *Appl. Phys. Lett.* **2010**, *96*, 012102.
- Sedra, A. S.; Smith, K. C. In *Microelectronic Circuits*; Oxford University Press: Oxford, 2004; pp 290–291.
- Xiong, F. In *Digital Modulation Techniques*; Artech House Publishers: Boston, MA, 2006; pp 99–205.
- Koo, S.-M.; Li, Q.; Edelstein, M. D.; Richter, C. A.; Vogel, E. M. Enhanced Channel Modulation in Dual-Gated Silicon Nanowire Transistors. *Nano Lett.* **2005**, *5*, 2519–2523.
- Dodabalapur, A.; Katz, H. E.; Torsi, L.; Haddon, R. C. Organic Heterostructure Field-Effect Transistors. *Science* **1995**, *269*, 1560–1562.
- Heinze, S.; Radosavljevic, M.; Tersoff, J.; Avouris, P. Unexpected Scaling of the Performance of Carbon Nanotube Schottky-Barrier Transistors. *Phys. Rev. B* **2003**, *68*, 235418.
- Ishigami, M.; Chen, J. H.; Cullen, W. G.; Fuhrer, M. S.; Williams, E. D. Atomic Structure of Graphene on SiO₂. *Nano Lett.* **2007**, *7*, 1643–1648.
- Ferrari, A. C.; Meyer, J. C.; Scardaci, V.; Casiraghi, C.; Lazzeri, M.; Mauri, F.; Piscanec, S.; Jiang, D.; Novoselov, K. S.; Roth, S.; Geim, A. K. Raman Spectrum of Graphene and Graphene Layers. *Phys. Rev. Lett.* **2006**, *97*, 187401.
- Calizo, I.; Miao, F.; Bao, W.; Lau, C. N.; Balandin, A. A. Variable Temperature Raman Microscopy as a Nanometrology Tool for Graphene Layers and Graphene-Based Devices. *Appl. Phys. Lett.* **2007**, *91*, 071913.
- Calizo, I.; Bao, W.; Miao, F.; Lau, C. N.; Balandin, A. A. The Effect of Substrates on the Raman Spectrum of Graphene: Graphene-on-Sapphire and Graphene-on-Glass. *Appl. Phys. Lett.* **2007**, *91*, 201904.
- Romyantsev, S.; Liu, G.; Stillman, W.; Shur, M.; Balandin, A. A. Electrical and Noise Characteristics of Graphene Field-Effect Transistors: Ambient Effects, Noise Sources and Physical Mechanisms. *J. Phys.: Condens. Matter* **2010**, *22*, 395302.